Arabian Journal of Chemistry (2022) **15**, 103757

King Saud University

Arabian Journal of Chemistry

www.ksu.edu.sa
www.sciencedirect.com

ORIGINAL ARTICLE

Effective removal of anionic dyes from aqueous solutions by novel polyethylenimine-ozone oxidized hydrochar (PEI-OzHC) adsorbent

Islam Elsayed [a], **Sunith Madduri** [a], **Emad M. El-Giar** [b], **El Barbary Hassan** [a,*]

[a] *Department of Sustainable Bioproducts, Mississippi State University, Box 9820 Mississippi State, MS 39762, United States*
[b] *School of Sciences, University of Louisiana at Monroe, Monroe, LA 71209, United States*

Received 30 November 2021; accepted 30 January 2022
Available online 03 February 2022

KEYWORDS

Hydrochar;
Ozone;
Polyethylenimine;
Organic contaminants;
Sorption;
Water treatment

Abstract The adsorption behavior of the anionic dyes Remazol Brilliant Blue R (RBBR) and Reactive Black 5 (RB5) from aqueous solutions by polyethylenimine ozone oxidized hydrochar (PEI-OzHC) was investigated. The adsorption capacities of both dyes increased with functionalization of PEI in the hydrochar adsorbent. The results of surface characterization (FTIR, BET, TGA, elemental analysis, and SEM) showed that PEI modification greatly enhanced the adsorbent surface chemistry with a slight improvement of adsorbent textural properties. In addition, the adsorption kinetics data showed an excellent adsorption efficiency as reflected in the high removal percentages of the anionic dyes. The Isotherm results indicated that RBBR and RB5 dye adsorption occurred via monolayer adsorption, and chemisorption was the rate-controlling step. The PEI-OzHC adsorbent possesses higher maximum Langmuir adsorption capacity towards RBBR (218.3 mg/g) than RB5 (182.7 mg/g). This increase in adsorption capacity is attributed to the higher number of functional groups in RBBR that interact with the adsorbent. This study reveals the potential use of adsorbents derived from pine wood hydrochar in municipal as well as industrial wastewater treatment. Furthermore, surface chemistry modification is proven as an effective strategy to enhance the performance of biomass-derived adsorbents.

1. 1. Introduction

The quality of drinking water plays an essential role for the health and safety of not only human beings but also animals and plants (Can, 2019; Hu et al., 2021). The last decade has witnessed a drastic global increase in the usage of water due to increased industrialization, urbanization, rapid human population growth, and more recently the COVID-19 pandemic (Chakraborty et al., 2021; Duttagupta et al., 2021). As a con-

* Corresponding author.
E-mail address: e.hassan@msstate.edu (E.B. Hassan).
Peer review under responsibility of King Saud University.

Production and hosting by Elsevier

https://doi.org/10.1016/j.arabjc.2022.103757
1878-5352

sequence of the increased water consumption, the levels of organic and inorganic pollutants such as pesticides, toxic metals, detergents, and dyes have increased sharply in all types of water resources (Can, 2019; Liu et al., 2019; Sun et al., 2020). Almost 1.6 million tons of dyes are fabricated annually to meet the industrial necessity and roughly 10–15% of this volume is disposed of as wastewater (Tan et al., 2015). Among these, organic dyes are considered the most significant source of water pollution (Mutembei et al., 2021). Reactive dyes are the most widely used ones in the textile industry especially the anionic dyes of Remazol Brilliant Blue (RBBR) and Remazol Reactive Black (RB5). In recent years, several studies were developed for the removal of organic dye pollutant from aqueous solutions (Hartikainen et al., 2016; Reghioua et al., 2021; Jawad et al., 2022a; Jawad et al., 2022b).

Accordingly, the recent years have witnessed an increased research toward the use of more efficient techniques and methods for the removal of these poisonous and hazardous dyes and pigments from all water resources including industrial wastewater (Dutta et al., 2021). The currently used techniques include filtration (Kornaros and Lyberatos, 2006), coagulation (Biswas et al., 2020), precipitation (Pohl, 2020), ion exchange (Edgar and Boyer, 2021), ozonation (Nakamura et al., 2017), reverse osmosis (Schroeder et al., 2021), advanced oxidation (Grcic et al., 2017), and adsorption (John et al., 2018). Each of these techniques has its own advantages and disadvantages. However, among these purification techniques, adsorption is considered the most efficient and economic one for the removal of a wide range of contaminants including organic dyes from both drinking water and wastewater (Barakan and Aghazadeh, 2021; Jawad et al., 2022a). Adsorption takes place when molecules (adsorbate) in a liquid bind themselves (either physically or chemically) to the surface of a solid substance (adsorbent).

Activated carbon is the most versatile and widely used carbon-based adsorbent in water and wastewater purification and recycling. This is mainly due to its large surface area, porous nature that allows high adsorption capacity, good thermal stability, variable surface chemical composition, and ability to easily modify its surface to accommodate more adsorbates (Begum, 2018; Wang et al., 2020d). Commercial activated carbon has been effectively used as an adsorbent for the removal of reactive dyes in wastewater (Mohd Nasir et al., 2021). Commercial activated carbon can be expensive (Rafatullah et al., 2013), therefore, a cheap alternative to activated carbon, hydrochar (HC) is both porous and has a surface that can also be modified (Azzaz et al., 2020). In addition, the many polar functional groups (e.g., carboxylic, lactone, phenol, and hydroxyl groups) that develop on the surface of the HC during the hydrothermal carbonization step make HC the most attractive among all carbon-based adsorbents used in drinking water as well as wastewater treatment (Azzaz et al., 2020). The presence of these functional groups not only make HC more selective toward specific pollutants, but also, and more importantly, helps with the addition (grafting) of other functional groups to the surface of HC (Chen et al., 2021). To further enhance the selectivity and/or reactivity of HC toward specific dyes and contaminants, several methods have been used to further modify the surface of pristine HC to introduce selective functional groups able to interact with reactive dyes. These modification methods include physical (e.g., ozone oxidation) (Sajjadi et al., 2019), chemical (modifications using acids or bases) (Wiedner et al., 2013), ultrasonic irradiation (Wang et al., 2020b), and impregnation with metals and metal oxides (e.g., TiO_2, MgO, Fe_3O_4, Fe_2O_3) (Mengting et al., 2021). Chemical modification of HC has two main objectives: carbonization and activation. These two objectives can be achieved simultaneously with an activating chemical agent. Achieving these two benefits has been reported to enhance the performance of the HC as an amendment or as a sorbent. Generally, chemical modification (activation) is performed either using an acid (e.g., H_3PO_4) or an alkali (e.g., KOH, NaOH) . Acid treatment increases the porosity of the HC and makes its surface more acidic. On the other hand, alkali pretreatment activates the HC through increasing the O-functional groups as well as the surface basicity (Jais et al., 2021).

Currently, the modification of the HC through the introduction of functional groups into the carbon frame has become a hot research topic. Amino modification of HC using Polyethylenimine (PEI) is a promising and environmentally friendly method of enhancing the adsorption activity of HC towards organic pollutants (Jiang et al., 2019b; Wang et al., 2020a). This is because PEI contains primary, secondary, and tertiary amine groups allowing it to interact with organic contaminants through electrostatic interactions and hydrogen bonding (Sun et al., 2016). Several research groups reported grafting of PEI on the surface of aerobic granules to increase its sorption for organic dyes and several cations and anions including heavy metal ions (Sun et al., 2011a; Wang et al., 2015; Godiya et al., 2019; Suzaimi et al., 2019; Wang et al., 2020c; Cho et al., 2021). In this study, a novel PEI- ozonized HC (PEI-OzHC) adsorbent has been synthesized successfully and used as an adsorbent for the removal of the anionic dyes RBBR and RB5 from aqueous solutions. To the best of our knowledge, no research has been reported on the study of the adsorption of RBBR and RB5 on the surface of PEI-modified ozone oxidized HC (PEI-OzHC). The PEI-OzHC adsorbent was characterized using FTIR, TGA, BET, pH_{pzc}, elemental analysis, and SEM. In addition, adsorption experiments were carried out to investigate the effects of solution pH, adsorbent dose, contact time, and initial RBBR and RB5 concentrations on the adsorption process.

2. Materials and methods

2.1. Chemicals and reagents

Analytical grade reagents, hydrochloric acid, sodium hydroxide, sodium chloride, lead nitrate, ethanol, Remazol Brilliant Blue R (RBBR, Sigma-Aldrich, CAS: 2580–78-1, Empirical formula $C_{22}H_{16}N_2Na_2O_{11}S_3$, MW: 626.54, Fig. 1a) and Reactive Black 5 (RB5, Sigma-Aldrich, CAS: 17095–24-8, Empirical formula $C_{26}H_{21}N_5Na_4O_{19}S_6$, MW: 991.8, Fig. 1b) were obtained from Sigma Aldrich. Solutions used in this study were prepared by using high purity deionized water (DI, 17.8 megohm-cm) purified with Thermo Scientific E-pure Water purification system. RBBR and RB5 stock solutions (1 g/L) were prepared by dissolving 1 g of each dye in 1 L of DI water. The concentrations of the stock solutions were further diluted and used throughout the experiments. The pH of the dye solution was adjusted using either 0.1 M HCl or 0.1 M NaOH.

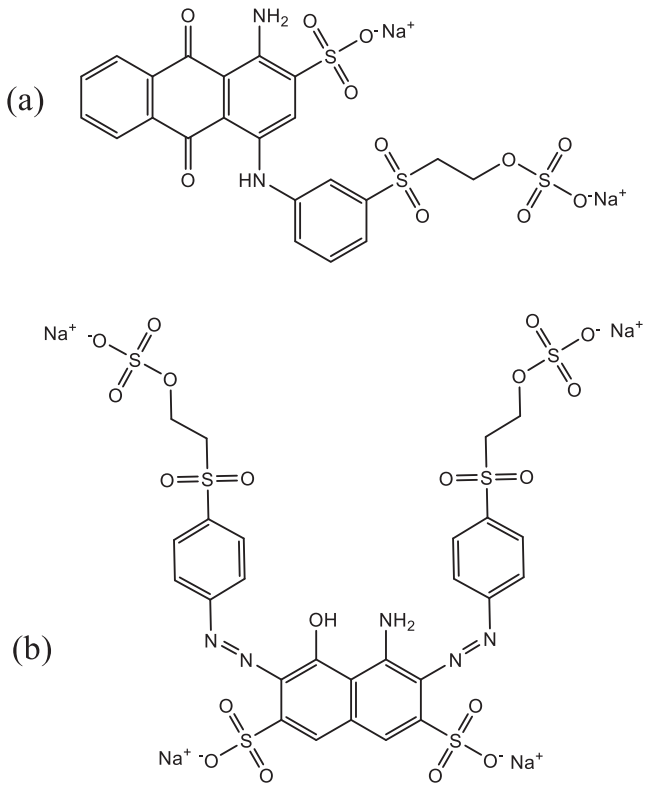

Fig. 1 Chemical structures of: (a) Remazol Brilliant Blue R (RBBR) and (b) Reactive Black 5 (RB5) dyes.

2.2. Hydrochar preparation

Pine wood biomass was used in this study as feedstock to prepare hydrochar. Dried pine wood chips (8–10% moisture content) were ground in a hammer mill. About 40 g of ground wood (< 20 mesh size) was mixed with 260 mL deionized (DI) water in 600 mL stainless steel autoclave of Parr reactor. The reactor was heated and held at 300 °C for 4 h with continuous stirring at 500 rpm. Then, the reactor was cooled to the ambient temperature and the hydrochar (HC) was collected. HC was washed several times with DI water to remove other impurities such as ash and dried at 100 °C in an oven. The dried HC was then ground to a uniform size in a pestle for homogeneity, stored in a sealed plastic bag, and its moisture content was determined for further experiments.

2.3. Hydrochar ozone oxidation and optimization

Hydrochar ozone oxidation was performed by Ozone Solutions generator (AZCO Industries VMUS-4S, CANADA). The oxidation experiments were performed in a cylindrical glass tube at room temperature at different times ranging from 60 to 360 min. Briefly, 3 g of dry hydrochar was added to the cylindrical glass tube. The experimental setup has an inlet connected to the ozone generator, which is first connected with an oxygen cylinder. The outlet of the glass tube cylinder was covered with quartz wool to prevent escaping of hydrochar during the flow. The oxygen flow rate was set to 3 L/min and the ozone flow rate was 5 L/min. After each experiment, the ozonized hydrochar (OzHC) samples were washed with DI water, dried overnight, and used for the determination of carboxylic content. The moisture content for the OzHC was determined on a separate portion of the sample. Conductometric titration was performed for each sample to determine the carboxylic content and accordingly the optimum time for ozone oxidation. The experiment with the optimum carboxylic content was repeated several times to prepare enough quantity from OzHC.

2.4. PEI modification of ozone oxidized hydrochar

Modification of the OzHC with PEI was performed similar to the previous studies (Sun et al., 2011b; Ma et al., 2014). A 20 g portion of each OzHC was added to 200 mL of 10% (w/v) PEI/methanol solution in a 500 mL conical flask. The PEI/methanol/ OzHC solution was agitated at 200 rpm for 24 h on an orbital shaker at 25 °C. The PEI-modified hydrochar was subsequently filtered and transferred to a 200 mL of 5% (w/v) glutaraldehyde solution for cross-linking. The solutions continued agitation at 200 rpm on an orbital shaker for 30 min. Finally, the PEI modified hydrochar was filtered and rinsed with deionized water and methanol to wash off any unreacted PEI, then dried at 100 °C overnight. The PEI-ozonized hydrochar (PEI-OzHC) was then stored in a sealed plastic bag for further use.

2.5. Characterization of the hydrochars

Raw HC and PEI-OzHC were grounded individually in a grinder to produce homogeneous samples. CE-440 Elemental Analyzer (Exeter Analytical, North Chelmsford, MA Carbon) was used to determine hydrogen, nitrogen, and oxygen content (by subtraction). Functional group analysis study was performed by using Thermo Scientific Nicolet iS50 FT-IR spectrometer in the range 400–4000 cm^{-1}. Thermogravimetric analyses (TGA) were performed using a Thermo Scientific SDT Q600 series Thermogravimetric Analyzer (TA instrument). The Surface morphology of all tested hydrochars was studied using a FE-SEM (JEOL JSM-6500F Field Emission Scanning Electron Microscope). Surface area, pore volumes, and pore diameters were determined by nitrogen adsorption–desorption isotherms at – 196 °C by a Quantachrome Autosorb iQ gas sorption analyzer (Quantachrome ASIQC0500-5, USA).

2.6. Surface acidity and point of zero charge (PZC) determination

Conductometric acid-base titrations were performed to determine the acidity of the PEI-OzHC. Briefly, a 0.5 g sample was suspended in 60 mL of 0.01 M NaCl solution using a mechanical stirrer and titrated against a standard 0.05 M NaOH solution. The pH and conductometric titration data were measured using an Oakton PC 2700 m. The PZC for PEI-OzHC was determined by mixing 50 mg samples with 25 mL portions of 0.01 M NaCl solutions pre-adjusted to pH 2, 4, 6, 8, 10 and 12 either using 0.1 M HCl or NaOH. Before mixing, the NaCl solutions were purged with N_2 gas to remove dissolved CO_2. The samples were agitated in a shaker for 24 h at room temperature and the pH of the filtered solutions were measured. The initial and final pH values were graphically plotted to evaluate the PZC.

2.7. Adsorption experiments

The adsorption performance of the PEI-OzHC was evaluated in a batch of RBBR and RB5 solutions. For both RBBR and RB5 adsorption, the influence of solution pH on adsorption performance was studied by adjusting the pH from 2 to 8 with one pH intervals using 0.1 M HCl and 0.1 M NaOH solutions. For this purpose, 30 mL of each solution was mixed with 10 mg of the PEI-OzHC. The dye solutions with adsorbents were placed in a shaker and agitated at 200 rpm for different time intervals ranging from 30 to −360 min. After agitation, the samples were filtered with a 0.22 μm syringe filter, and the dye concentrations in the filtrate were determined using a Variant UV Spectrophotometer at wavelength ~ 597 nm and ~ 593 nm, respectively. The adsorption capacity of the PEI-OzHC was determined using the following equation:

$$q_t = \frac{(C_0 - C_t) \times V}{m} \quad (1)$$

where C_0 and C_t (mg/L) are the initial and final concentrations of dyes at time t, respectively, V is the volume of adsorbate solution (L), and m (g) is the dry weight of hydrochar.

Kinetic adsorption experiments were conducted by mixing 10 mg of the PEI-OzHC with 30 mL of aqueous dye solutions of different initial concentrations (75,100 and 125 mg/L for RBBR and 50, 75 and 100 mg/L for RB5) at pH 6 and 30 °C. The samples were placed in a shaker at 200 rpm for different time intervals ranging from 30 to 360 min. The samples were withdrawn at respective time intervals and filtered. The concentrations of each dye in the filtrate were determined using the UV Spectrophotometer and the adsorption capacity was determined using Eq. (1).

Isotherms adsorption experiments were conducted by mixing 10 mg of the PEI-OzHC with 30 mL of dye solutions with different concentrations (5–1000 mg/L) at pH 6. The samples were placed in the orbital shaker at 200 rpm for 4 h at different temperatures of 15, 30, and 45 °C. At the end of each experiment, the samples were filtered, and the adsorption capacity was determined by using Eq. (1) as well.

3. Results and discussions

3.1. Ozone optimization of hydrochar

First, the highest carboxylic functional groups in the OzHC was determined by time optimizing experiment. To achieve this, a series of exploratory experiments were performed by changing the ozonolysis time from 60 to 360 min (Fig. 2). The carboxylic content of the raw HC (70 μmol/g) was increased to 116 μmol/g after 60 min ozonolysis. Further increase in the ozonolysis time led to gradual increase in the carboxylic content of OzHC till reached maximum (272.6 μmol/g) after 240 min. This increase in the carboxylic content can be attributed to the cleavage and oxidation of certain (C = C) double bonds in the hydrochar (Kharel et al., 2019). The OzHC can be oxidized through the electrophilic ozonolysis mechanism of (C = C) double bonds in three steps as proposed by Gómez et al. (Gómez-Serrano et al., 2002). Any further increase in the ozonolysis time beyond 240 min had no effect on the carboxylic content indicating the maximum oxidation capacity. Accordingly, 240 min was determined as the optimum ozonolysis time in this study to produce PEI-OzHC.

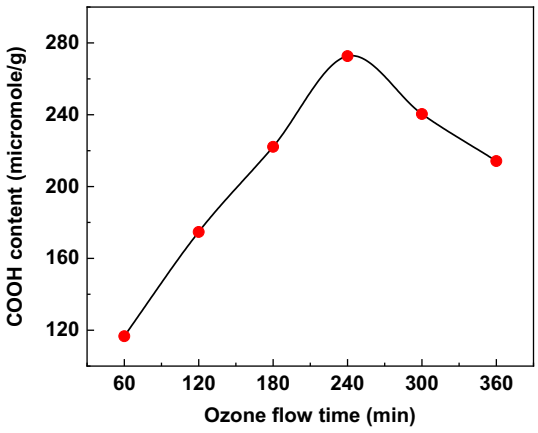

Fig. 2 Effect of ozone time flow on the COOH content of OzHC.

3.2. Characterization of raw and PEI-modified hydrochar

Combustion elemental composition and surface area results for both HC and PEI-OzHC are presented in Table 1. The N content in the PEI-OzHC (9.31%) was almost twenty-five times higher than N content in HC (0.38). This result indicates successful grafting of amine functional groups on the surface of OzHC (Li et al., 2020). The specific surface area of PEI-OzHC was slightly decreased from 5.209 to 3.764 m^2/g after the PEI grafting step. The decrease in surface area of PEI-OzHC can be attributed to either partial filling of pores by PEI or aggregation of PEI on the surface of the OzHC as suggested by (Lv et al., 2018).

Fig. 3a, shows the FTIR spectra of the major functional groups exist in both raw HC and PEI-OzHC. The broad absorbance band around 3400 cm^{-1} belongs to O–H stretching vibration of hydroxyl groups indicating the presence of alcohols and phenols on the hydrochar surface. The intensity of this band was more pronounced in PEI-OzHC due to its overlap with N—H bending vibration band (Wang et al., 2020e). The bands at 2935 and 2860 cm^{-1} are attributed to C—H stretching vibration in methyl and methylene groups. The band at 1690 cm^{-1} of raw HC is consistent with C═O stretching vibrations of carboxylic acids and aldehydes. The strong peak at 1665 cm^{-1} of PEI-OzHC can be attributed to the stretching vibration of C═O of amides or C═N of imines. The peaks at 1450 and 1350 cm^{-1} were mainly assigned to C—N stretching vibration (Ma et al., 2014; Jawad et al., 2020). The stretching bands at 1265 and 1208 cm^{-1} corresponds to the vibration of C—O—C bonds (Wang et al., 2020e). The peak at 1033 cm^{-1} corresponds to the stretching vibrations of the C-O bonds of ethers, alcohols, phenols, and esters (Jawad et al., 2021). All the above FT-IR results suggests successful oxidation and grafting of PEI on the surface PEI-OzHC (Chen and Huang, 2010).

Thermalgravimetric analysis (TGA) was performed on both raw HC and PEI-OzHC to examine their thermal stabilities. The weight loss versus temperature for both raw HC and

Table 1 Elemental analysis and surface area of OzHC and PEI-OzHC.

Treatment	Elemental analysis						Surface area(m^2/g)
	%C	%H	%N	%O	Molar N/C	Molar O/C	
Raw HC	73.44	5.21	0.38	20.97	0.005	0.285	5.209
PEI-OzHC	62.33	5.2	9.31	23.16	0.149	0.371	3.764

PEI-OzHC from room temperature to 800 °C are shown in Fig. 3b. For raw HC, the experienced weight loss below 150 °C is due to desorption of moisture and gasses. The obvious weight loss occurred between 150 and 450 °C can mainly attributed to the decomposition of oxygen containing compounds introduced during the hydrothermal carbonization step (Abdulhameed et al., 2021). The weight loss shown after 450 °C is mainly due to the decomposition of lignin (Ocampo-Perez et al., 2019). PEI-OzHC contains substantial amounts of oxygenated and amine-functionalized compounds that was introduced during both ozonolysis and PEI grafting steps, these compounds start to degrade at temperatures between 150 and 450 °C (Wang et al., 2020e). As a result, PEI-OzHC showed more significant and rapid weight loss compared with OzHC in this temperature region. The first pronounced weight loss peak obtained at 300 °C was mainly due to the decomposition of oxygen containing compounds and the second weight loss peak obtained at 400 °C can be attributed to the decomposition of the grafted PEI molecules in on the surface of OzHC (Roy et al., 2015; Jiang et al., 2019a).

FE-SEM analysis of HC (Fig. 3C) and PEI-OzHC (Fig. 3d) show the differences in morphology and structures of both hydrochars. It is obvious that morphology of raw (HC) was drastically changed after ozone and PEI grafting steps. The image of raw HC displays smooth disrupted surface with holes which transformed into rough and irregular surface structure after ozone-PEI modification. This could be due to the introduction of carboxylic and amino groups on the HC surface and PEI can clearly be seen on the surface of PEI-OzHC as indicated in the previous studies (Wang et al., 2020e). This confirms the occurrence of some sort of interaction between active sites of HC and Ozone-PEI functionalities.

Fig. 3e and 3f show the Nitrogen adsorption isotherm and average pore size distribution for the PEI-OzHC. PEI-OzHC sample demonstrated type III isothermal curves indicating that the material has nonporous or macroporous structure due to the destruction of porous structure as a result of the oxidation process. The nitrogen BET surface areas for HC and PEI-OzHC were 5.209 and 3.764 m^2/g respectively (Table 1). The slight decrease in surface area could be attributed to the incorporation of PEI on the biochar surface. This decrease in surface area of PEI-OzHC indicates that any improve in the adsorption process will be mainly related to the chemical interaction between the functional groups of both adsorbent and adsorbate.

3.3. Adsorption study

3.3.1. Effect of solution pH on RBBR and RB5 adsorption

Preliminary sorption tests were carried out on raw HC for both RBBR and RB5. The adsorption capacity was extremely low and accordingly no further studies were performed on raw HC. The pH of the dye solution generally acts as a crucial factor in determining the sorption capacities of sorbent towards the dye molecules. The pH specifically impacts the accessibility of solute towards a specific functional group by altering the surface chemistry of the sorbent. The H^+ ion concentration in the solution determines both the surface charge of the adsorbent and the types of the ion in the solution to be adsorbed. The surface charge of the adsorbent also changes as the H^+ ion concentration changes in the solution. Therefore, it is important to determine the adsorbent surface charge and the point of zero charge (PZC) where the surface charge is zero (Madduri et al., 2020). For this purpose, the adsorbent was equilibrated with solutions having different pH and same ionic strength without dyes. The final pH of each solution was measured, and the adsorbent surface charge was determined and represented in Fig. 4a. The PZC for PEI-OzHC adsorbent was determined at 5.7 pH implying the presence positive charge on the adsorbent surface below this pH and negative charge above this pH. Therefore, the maximum adsorption capacity for anionic dyes such as RBBR and RB5 is expected to be high at pH $<$ 5.7 due to the high electrostatic interaction between adsorbent and adsorbate (Jawad et al., 2019). To investigate the effect of pH on the adsorption of RBBR and RB5 dyes, adsorption of both dyes on the surface of PEI-OzHC was performed at different initials pH and the obtained results were represented in Fig. 4b. As shown in the figure, the adsorption capacity for both dyes rapidly deceased at high acidic conditions (pH = 2–6), then slightly decreased after pH = 6. At lower pH (pH = 2–3), the high concentration of H^+ in the solution will result in more protonation for amine groups on PEI-OzHC surface forming positively charged sites ($-NH_3^+$) which increase the electrostatic interaction with the sulfonic acid groups of both dyes and consequently increase the adsorption. As pH increase (pH = 2–6), protonation of amine groups would be weakened and the electrostatic interaction would be reduced, which lead to reduction in the adsorption capacity of PEI-OzHC (Li et al., 2019). The adsorption of both dyes decreases gradually with increasing the pH and reaches minimum at pH = 8 because the surface of the PEI-OzHC becomes negatively charged. As it is more economic to study the adsorption behavior near neutral pH, therefore, we studied the adsorption behavior of both dyes slightly above the PZC at pH = 6. This pH was frequently reported to be ideal for anionic dyes removal (Ergene et al., 2009; Mate and Mishra, 2020). It is worthy to note that, at the same studied pH, the adsorption capacity for RBBR dye with two sulfonic acid groups was higher than adsorption capacity of RB5 with four sulfonic acid groups as indicated in Fig. 1. This result could be probably attributed to the relatively small MW and size of RBBR dye which allow more adsorption for dye on the surface of PEI-OzHC. Our results are in good agreement with the previous results reported by (Munagapati et al.,

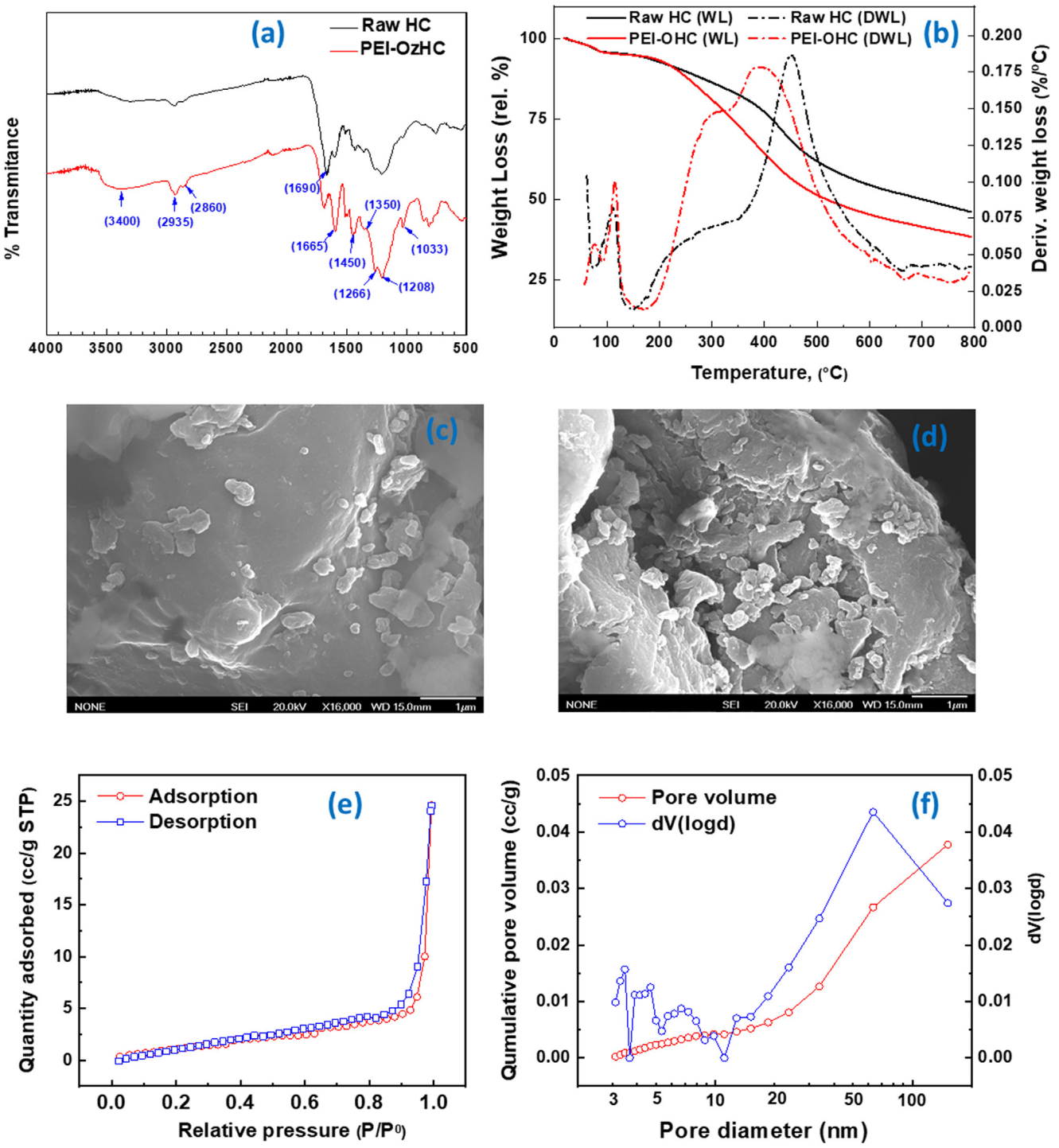

Fig. 3 (a) FTIR spectra of raw (HC) and PEI-OzHC, (b) TGA-DTG thermograph of raw (HC) and PEI-OzHC, (c) FE-SEM micrographs of the raw (HC), (d) FE-SEM micrographs of (PEI-OzHC), (e) and (f) Nitrogen adsorption–desorption isotherms at −196 °C and the corresponding average pore size distribution for the PEI-OzHC.

2018) which indicated RBBR dye (MW = 696.665 g/mol) has higher adsorption capacity than RB5 dye (MW = MW: 991.8) at the same concentration of dye. This result also indicates that the adsorption process of dyes on the PEI-OzHC surface are not only dependent on the electrostatic interaction between dyes and adsorbents, but also depends on the size and molecular weight of the dye.

3.3.2. Adsorption kinetics

The kinetic study is an important aspect of any adsorption process in order to better understand the mechanism involved during the process. Understanding kinetics also has great significance for pilot plant applications. In order to investigate the mechanism and determine adsorption rate constant of RBBR and RB5 dyes onto PEI-OzHC surface, three kinetic

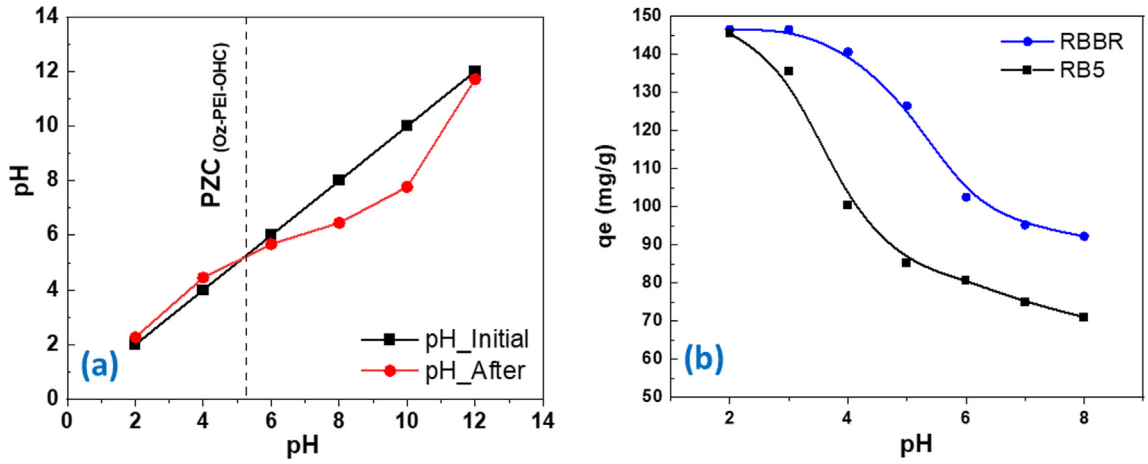

Fig. 4 (a) Determination point of zero charge (PZC) for the PEI-OzHC, (b) Effect of different pH on RBBR and RB5 adsorption.

models of pseudo-first order, pseudo-second order, and Elovich were used in this study.

The pseudo-first order model (Lagergren, 1898) is expressed as:

$$q_t = q_e(1 - e^{-K_1 t}) \tag{2}$$

where q_e (mg/g) is the adsorption capacity at equilibrium, q_t (-mg/g) is the adsorption capacity at time t, and k_1 (min^{-1}) is the rate constant of pseudo-first order adsorption.

The pseudo-second order model (Ho and McKay, 1999) is expressed as:

$$q_t = \frac{q_e^2 k_2 t}{1 + q_e K_2 t} \tag{3}$$

where k_2 (g/(mg min)) is the rate constant of pseudo-second order adsorption.

The Elovich model (Peers, 1965) is expressed as:

$$q_{t=\frac{1}{\beta}\ln(1+\alpha\beta t)} \tag{4}$$

where α (mg/g*min) is the initial adsorption rate; and β (mg/g) is the desorption constant.

The effect of contact time on RBBR and RB5 adsorption onto PEI-OzHC at 25 °C was determined, and the data were correlated by the above three kinetic models as shown in Fig. 5. It is clear from the figure that the adsorption capacity of both dyes is strongly dependent on the initial concentration of the dye, high adsorption occurred at high concentration of the dye. For example, the adsorption capacity of RBBR was increased from 109.2 to 131.2 mg/g with changing the concentration from 75 to 125 mg/L as indicated in Table 2. The results also indicated that adsorption rates of both dyes were significantly fast within the first 60 due to the higher concentration of the dyes and the availability of more adsorption active sites on the hydrochar surface. As the time increased, less active sites of PEI-OzHC becomes available to bind with the low concentrated dye molecules and this would lead to decline in sorption rate until the equilibrium is achieved within 180 min for both dyes (Senthilkumar et al., 2018). The calculated kinetic parameters of adsorption capacity ($q_{e,\ exp}$), corresponding rate constants, correlation coefficients (R^2), and chi-square (X^2) values for both RBBR and RB5 dyes are presented in Tables 2 and 3, respectively. As it can be observed, the correlation coefficients values of the pseudo-second order kinetic model ($R^2 > 0.999$) are higher than those in the pseudo-first order and Elovich models for both dyes. Pseudo-second order model also showed low chi-square (X^2) error value compared with other models. Moreover, the adsorption capacity values calculated by the pseudo-second order kinetic model ($q_{e,\ cal}$) were very close to the experimental adsorption capacities ($q_{e,\ exp}$) values (Madduri et al., 2020). Therefore, pseudo-second order model was chosen to explain the adsorption of RBBR and RB5 dyes onto PEI-OzHC hydrochar. It is clear that the best fit kinetic model was selected by its goodness of fit, correlation coefficient (R^2) and Chi-square (χ^2) value. Accordingly, the adsorption capacity of RBBR and RB5 dyes onto the PEI-OzHC is proportional to the number of active sites occupied in the adsorbent and the concentration of the dye. The rate coefficient, k_2 of pseudo-second order for RBBR and RB5 dyes were found to increase with an increase in initial dye concentration. This could be due to fast sorption kinetics at higher concentrations. The adsorption of similar anionic dyes such as RB5 and Congo red dyes on onto banana peel powder was also reported to follow the pseudo-second order kinetic model (Munagapati et al., 2018).

3.3.3. Adsorption isotherms

The equilibrium adsorption isotherms can provide the most promising data to understand the mechanism of adsorption and the interaction between both adsorbent and adsorbates (Mate and Mishra, 2020). In this study, three different isotherm models (Langmuir, Freundlich, and Sips) were chosen to predict the adsorption capacities and to fit the experimental equilibrium data. The Langmuir adsorption isotherm (Langmuir, 1918) is used to estimate the maximum adsorption capacity at equilibrium corresponding to complete monolayer coverage of adsorbate on adsorbent surface. Langmuir isotherm equation can be expressed as:

$$Q = \frac{Q_{max} b_L C_e}{1 + b_L C_e} \tag{5}$$

where Ce (mg/L) is the solution concentration at equilibrium, q_e (mg/g) is the equilibrium adsorption capacity, q_{max} (mg/g) is the maximum adsorption capacity, and b is the Langmuir adsorption constant related to adsorption energy. The essential

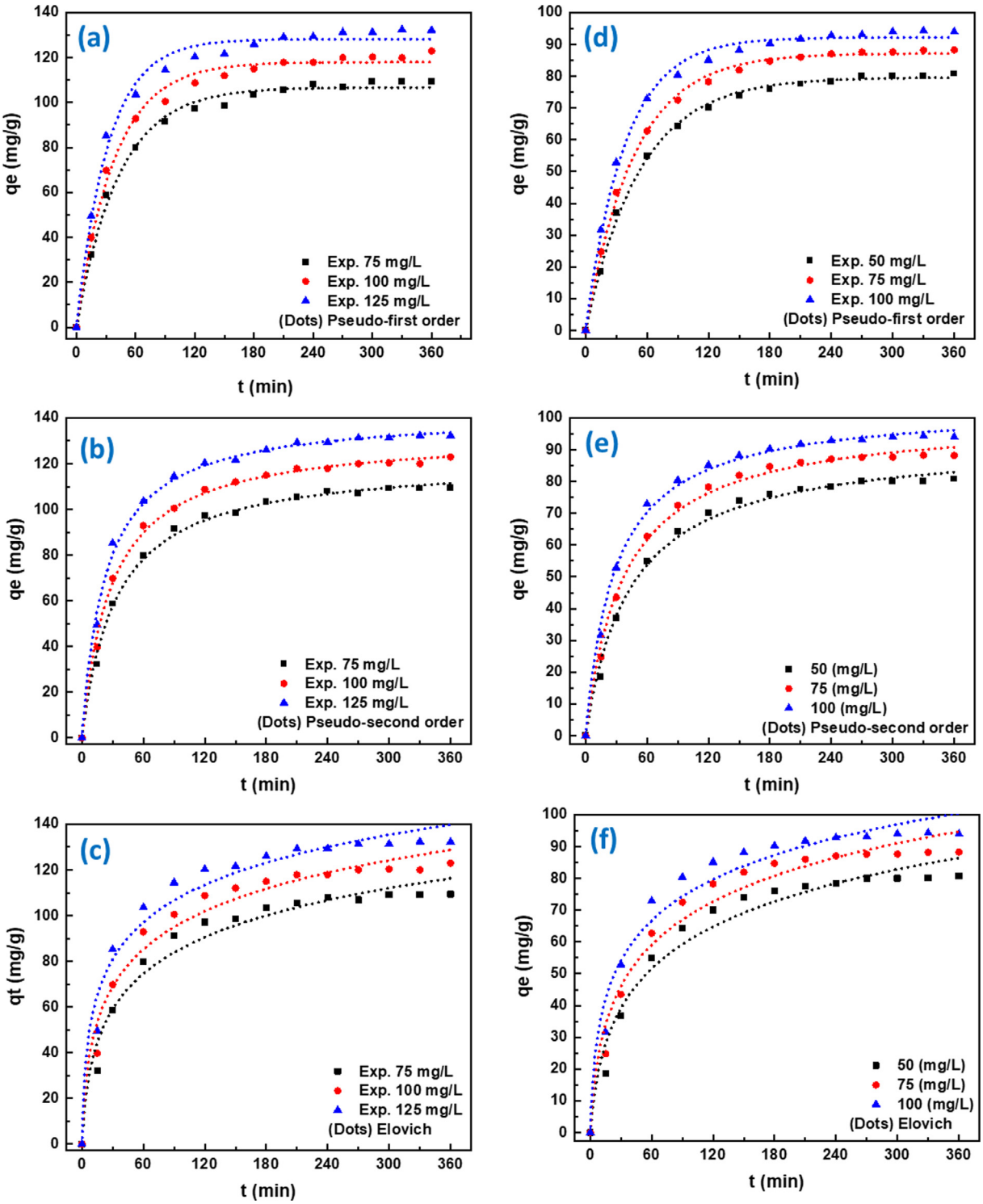

Fig. 5 Adsorption kinetic curves of RBBR (a-c) and RB5 (d-f) dyes at 25 °C: Experimental results and non-linear fitting of pseudo-first order (a,d), pseudo-second order (b,e), and Elovich model (c,f).

characteristic of Langmuir isotherm can be expressed in terms of a dimensional equilibrium parameter (R_L) (Ho et al., 1996) according to the following equation:

$$R_L = \frac{1}{1 + K_L C_0} \tag{6}$$

where K_L is the Langmuir constant (L/mg) and C_0 is the initial adsorbate concentration (mg/L).

Freundlich isotherm is applicable to adsorption processes that occur on heterogonous surfaces and it defines the surface heterogeneity and the exponential distribution of active sites

Table 2 Kinetic parameters for RBBR dye adsorption.

Model	Parameter	C_o (mg/L)		
		75	100	125
Pseudo-first order	q_e, exp (mg/g)	109.2	120.0	131.2
	q_e, calc (mg/g)	106.7	118.0	128.2
	K_1 (1/min)	0.023	0.026	0.031
	R^2	0.993	0.990	0.987
	X^2	7.60	12.30	18.94
Pseudo-second order	q_e, exp (mg/g)	109.2	120.0	131.2
	q_e, calc (mg/g)	120.2	131.5	140.9
	K_2 (g/mg min)	$2.46x10^{-4}$	$2.60x10^{-4}$	$3.03x10^{-4}$
	R^2	0.999	0.999	0.999
	X^2	2.07	1.67	1.74
Elovich	q_e, exp (mg/g)	109.2	120.0	131.2
	α (mg/g min)	8.66	12.69	22.38
	β (g/mg)	0.042	0.041	0.042
	R^2	0.970	0.971	0.970
	X^2	32.71	37.65	44.56

and their energies (Ayawei et al., 2015). Freundlich isotherm equation (Freundlich and Helle, 1939) can be expressed as:

$$Q = K_F C_e^{1/nF} \tag{7}$$

where K_F is the adsorption capacity (L/mg) and 1/n is the adsorption intensity; it also indicates the relative distribution of the energy and the heterogeneity of the adsorbate sites.

Sips model is a hybrid form of the Langmuir and Freundlich expressions for heterogeneous adsorption systems. This circumvented the limitation of the rising adsorbate concentration associated with Freundlich isotherm model. At low adsorbate concentrations, the Sips model reduces to the Freundlich isotherm; at high concentrations, it predicts a monolayer adsorption capacity characteristic of the Langmuir isotherm. The Sips parameters are governed mainly by the operating conditions such as the pH, temperature and concentration (Foo and Hameed, 2010). Sips model (Sips, 1948) can be expressed as:

$$\frac{1}{qe} = \frac{1}{q_{max} K_s} \left(\frac{1}{ce}\right)^{\frac{1}{ns}} + \frac{1}{q_{max}} \tag{8}$$

where K_s is the Sips equilibrium constant (1/mg), q_{max} is the Sips maximum adsorption capacity (mg/g), and n_s is Sips model exponent which can be employed to describe the system's heterogeneity when n_s is between 0 and 1.

The isotherm studies of RBBR and RB5 dyes were investigated at three different temperatures 15, 30, and 45 °C and the results are shown in Fig. 6. Adsorption isotherms for RBBR and RB5 dyes were fitted to Langmuir (6a, d), Freundlich (6b, e), and Sips (6c, f) isotherms using non-linear regression. Tables 4 and 5 present the linear fitting parameters of Langmuir, Freundlich, and Sips isotherm models. For both RBBR and RB5 dyes, the maximum adsorption capacity (q_m) of Langmuir isotherm was found to increase by applying high temperature. It increased from 148.2 to 217.3 mg/g for RBBR dye and from 99.5 to 182.7 mg/g for RB5 dye, respectively, and this could be attributed to a rise in kinetic energy of the sor-

Table 3 Kinetic parameters for RB5 dye adsorption.

Model	Parameter	C_o (mg/L)		
		50	75	100
Pseudo-first order	q_e, exp (mg/g)	80.2	88.2	94.0
	q_e, calc (mg/g)	79.6	87.2	92.2
	K_1 (1/min)	0.018	0.021	0.026
	R^2	0.998	0.997	0.995
	X^2	1.31	1.73	3.96
Pseudo-second order	q_e, exp (mg/g)	80.2	88.2	94.0
	q_e, calc (mg/g)	91.9	99.2	102.7
	K_2 (g/mg min)	$2.66x10^{-4}$	$2.88x10^{-4}$	$3.70x10^{-4}$
	R^2	0.999	0.999	0.999
	X^2	2.60	2.40	1.63
Elovich	q_e, exp (mg/g)	80.2	88.2	94.0
	α (mg/g min)	4.00	5.78	10.19
	β (g/mg)	0.049	0.048	0.052
	R^2	0.968	0.968	0.967
	X^2	21.04	23.82	26.52

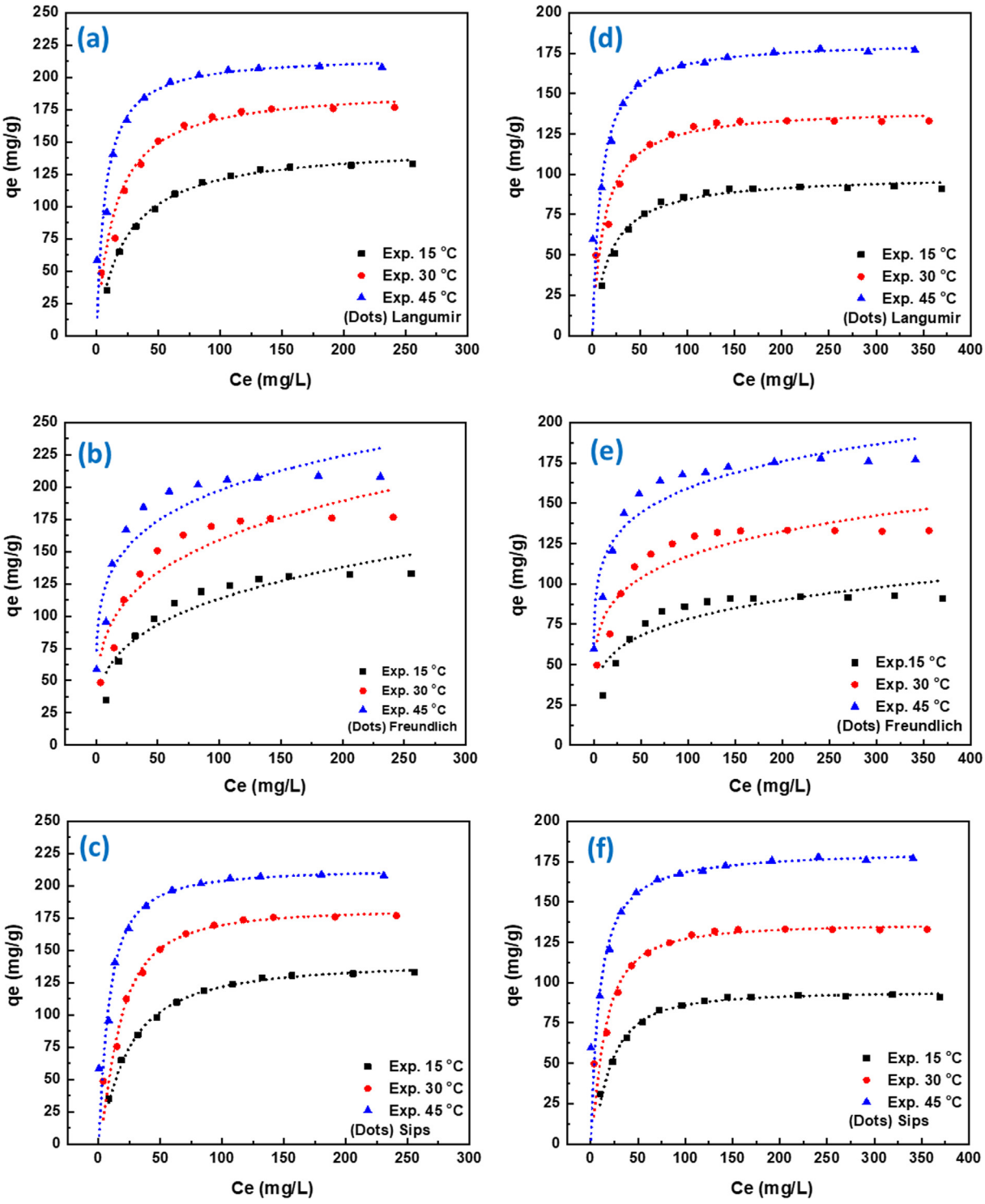

Fig. 6 Adsorption isothermal curves of RBBR (a-c) and RB5 (d-f) dyes at different temperatures: Experimental results and non-linear fitting of Langumir model (a,d), Freundlich model (b,e), and Sips model (c,f).

bent particles due to the rise in temperature (Munagapati et al., 2018). The correlation coefficient of linear form of Langmuir model shows a very good fit to the experimental data (R^2 = 0.999). In addition, the values of R_L which calculated from Eq. (6) are in the range of 0–1, which indicates favorable monolayer adsorption of RBBR and RB5 dyes onto PEI-OzHC. The Freundlich isotherm constant K_F was increased from 31.0 to 84.5 mg/g for RBBR dye and from 30.7 to 81.9 mg/g for RB5, respectively, with increase the temperature of the adsorption. This increase in K_F with temperature confirming again that the adsorption process of both dyes is endothermic. The 1/n values were found in the range 0–1

Table 4 Adsorption isotherms parameters for RBBR dye adsorption.

Model	Parameter	Temperature		
		15 °C	30 °C	45 °C
Langmuir	q_m (mg/g)	148.2	192.1	217.3
	K_L (L/mg)	0.044	0.070	0.146
	R^2	0.999	0.999	0.999
	X^2	3.36	10.87	3.43
Freundlich	K_F (mg/g) (L/mg)$^{1/n}$	31.00	49.87	84.56
	n_F	3.55	3.97	5.43
	R^2	0.879	0.859	0.884
	X^2	123.5	280.2	303.9
Sips	q_{max} (mg/g)	150.15	195.7	218.3
	K_s ((L/mg)	0.169	0.021	0.077
	n_s	0.691	0.817	0.820
	R^2	0.999	0.999	0.999
	X^2	4.84	1.90	2.51

Table 5 Adsorption isotherms parameters for RB5 dye adsorption.

Model	Parameter	Temperature		
		15 °C	15 °C	15 °C
Langmuir	q_m (mg/g)	99.46	141.0	182.7
	K_L (L/mg)	0.056	0.081	0.115
	R^2	0.999	0.999	0.999
	X^2	5.72	8.73	3.06
Freundlich	K_F (mg/g) (L/mg)$^{1/n}$	30.71	51.90	81.94
	n_F	4.92	5.65	6.92
	R^2	0.784	0.830	0.813
	X^2	79.15	127.7	120.5
Sips	q_{max} (mg/g)	94.46	136.7	181.9
	K_s ((L/mg)	0.012	0.027	0.101
	n_s	0.687	0.747	0.859
	R^2	0.999	0.999	0.999
	X^2	1.95	6.27	3.31

Table 6 Adsorption capacity of different modified hydrochar and biochar adsorbents towards RBBR dyes in aqueous solutions.

Adsorbent	Adsorbate	pH	q_{max} (mg/g)	Reference
Ozone-PEI Hydrochar	RBBR	6.0	218.3	**This study**
Coconut coir Activated carbon		6.9	15.2	(Kavitha and Namasivayam, 2008)
Orange peel Biochar		–	11.6	(Mafra et al., 2012)
Corn cob activated carbon		6	12.6	(Ahmada aet al., 2011)
Sewage activated carbon		2	33.5	(Silva et al., 2016)
HNO_3 Activated carbon		3	23.6	(Dağdelen et al., 2014)
Seaweed Biochar		2	92.5	(Vijayaraghavan and Ashokkumar, 2019)
Commercial Activated carbon		3	199.4	(Dağdelen et al., 2014)
H_2O_2 treated biochar		5.9	357	(Nair and Vinu, 2016)
Peanut hull-based H_3PO_4 activated carbon		–	149.25	(Zhong et al., 2012)
Epichlorohydrin Walnut shell biochar		2	224.4	(Li et al., 2019)
H_3PO_4 Biomass		2	292	(Silva et al., 2018)
Pomegranate peel activated carbon		2	370.9	(Ahmad et al., 2014)

Table 7 Adsorption capacity of different modified hydrochar and biochar adsorbents towards RB5 dyes in aqueous solutions.

Adsorbent	Adsorbate	pH	q_{max} (mg/g)	Reference
Ozone-PEI Hydrochar	RB5	6.0	182.7	**This study**
Fe_3O_4 Biochar		10	2.9	(Khan et al., 2015)
Macadamia Seed biochar		3	1.1	(Felista et al., 2020)
Candida tropicalis char		3	101.9	(Donmez, 2001)
Cu–Cu_2O Biochar		9	5.4	(Khan et al., 2015)
PEI with coffee waste Biochar		7	77.5	(Wong et al., 2020)
Banana peel biochar		3	49.2	(Munagapati et al., 2018)
Date seed biochar		2	113.4	(Senthilkumar et al., 2018)

(0.28–0.18 for RBBR, and 0.20–0.18 for RB5) indicating that the adsorption of both dyes is favorable under the applied conditions. The low correlation coefficients (R^2) and the high Chi-square (X^2) values of Freundlich isotherm suggesting the weakness of this model in explaining adsorption process. The Sips isotherm constant q_{max} was increased from 150.1 to 218.3 mg/g for RBBR dye and from 94.5 to 181.9 mg/g for RB5, respectively, with increase the temperature of solution from 15 to 45 °C. The Sips q_{max} values were very similar to the values obtained by Langmuir isotherm. The values of n_s are in the range of 0–1 which again indicates the heterogeneity of the surface of the adsorbent. The higher correlation coefficients values (R^2 = 0.999) and the low Chi-square (X^2) values of Sipes isotherm suggesting the suitability of this model in explaining adsorption process. The overall results suggesting that Langmuir and Sips isotherm to be the best fitting models for the adsorption isotherms data of RBBR and RB5 dyes onto PEI-OzHC. Both models displayed the closest maximum adsorption capacity (q_m) with experimental data, highest correlation coefficient (R^2) and the lowest Chi-square (X^2) values. Several adsorption studies of anionic dyes were also reported to follow Langmuir and Sips adsorption models (Munagapati et al., 2018; Fernandes et al., 2020). The adsorption capacities in this study was higher than, or comparable with other previous studies which used modified biochar or hydrochar as adsorbents as shown in Tables 6 and 7).

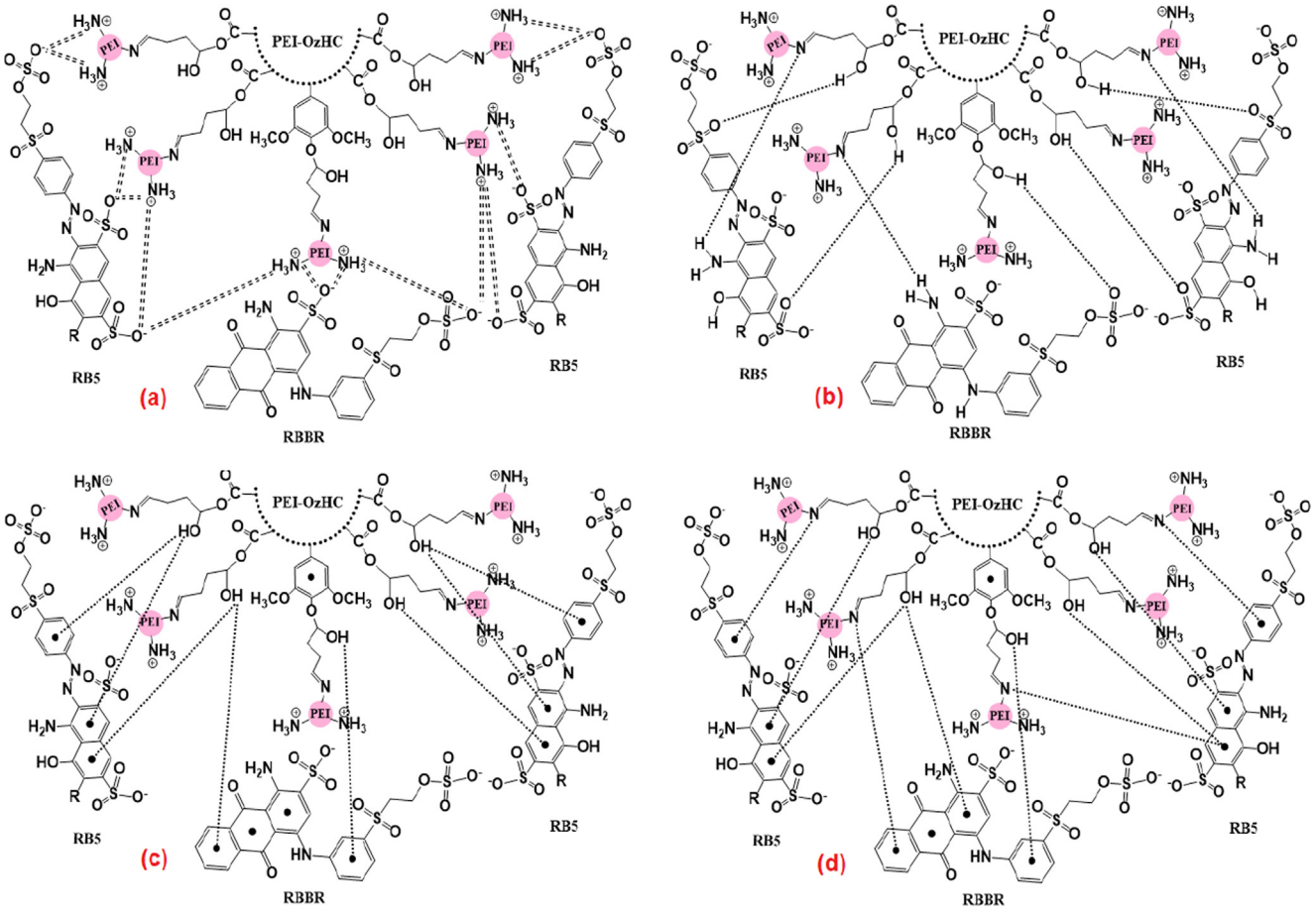

Fig. 7 Illustration of the possible adsorption mechanism between PEI-OzHC and (RBBR, RB5) dyes: a) electrostatic attraction, b) hydrogen bonding, c) Yoshida H-bonding, and d) n–π interaction.

3.3.4. Adsorption mechanism

Fig. 7 represents the adsorption mechanism of RBBR and RB5 dyes onto the surface of PEI-OzHC adsorbent relying on the presence of different functional groups and charges on both adsorbent and adsorbates. At pH < 5.7, the electrostatic attraction between amino groups on PEI-OzHC adsorbent and the sulfonate groups on RBBR and RB5 adsorbates can be occurred due to the good distribution of cationic amino group (NH_3^+) on the surface of the adsorbent as shown in Fig. 7a. Furthermore, the presence of the hydrogen bonding between the free hydrogen, oxygen, and nitrogen in both PEI-OzHC adsorbent and RBBR and RB5 adsorbates molecular structures as seen in Fig. 7b. Also, the formation of Yoshida H-bonding interaction (Fig. 7c) between the hydrogen of hydroxyl groups on PEI-OzHC adsorbent and the aromatic rings on the RBBR and RB5 dyes can also be present. Eventually, another factor that can affect the adsorption mechanism is n–π interaction between the oxygen and nitrogen as electron-donating groups on the PEI-OzHC adsorbent surface and the π-system in the aromatic rings of RBBR and RB5 dyes as electron acceptor, Fig. 7d. To conclude, the adsorption mechanism has been controlled by four different factors including electrostatic attraction, hydrogen bonding, Yoshida H-bonding, and n–π interaction (Jawad et al., 2020; Malek et al., 2020).

4. Conclusions

In this study, a novel low-cost adsorbent was prepared by modification of Ozone oxidized hydrochar with PEI to introduce more amino groups on the hydrochar surface. The results indicated that Ozone oxidation improved the carboxylic content on the hydrochar and further modification with PEI significantly increased the amino groups which improved the adsorption performance for RBBR and RB5 removal. The adsorption process of both adsorbates was influenced by changing the pH and adsorption have occurred at neutral pH. Kinetics for the adsorption was considerably fast and kinetic adsorption data for both RBBR and RB5 were fitted well by the pseudo second-order model. Adsorption isotherms of RBBR and RB5 onto PEI-OzHC agree well with both Langmuir and Sips adsorption model. The maximum adsorption capacity (Q_{max}) determined from Langmuir isotherm model of RBBR and RB5 were 218.3 mg/g, and 182.7 mg/g, respectively at 45 °C. With increasing temperature, the adsorption capacities increased showing an endothermic nature and increase in favorable nature of adsorption. Ozone-PEI modification could be a viable method to tune the hydrochar surface with carboxylic and amino functionalities to create alternative and value-added adsorbents for environmental applications.

Declaration of Competing Interest

The authors declare that they have no known competing financial interests or personal relationships that could have appeared to influence the work reported in this paper.

Acknowledgment

This publication is a contribution of the Forest and Wildlife Research Center, Mississippi State University.This publication is also based upon work that supported by the National Institute of Food and Agriculture, U.S. Department of Agriculture, McIntire Stennis project under accession number 1012125.

References

Abdulhameed, A.S., Firdaus Hum, N.N.M., Rangabhashiyam, S., Jawad, A.H., Wilson, L.D., Yaseen, Z.M., Al-Kahtani, A.A., Alothman, Z.A., 2021. Statistical modeling and mechanistic pathway for methylene blue dye removal by high surface area and mesoporous grass-based activated carbon using K_2CO_3 activator. J. Environ. Chem. Eng. 9, 105530.

Ahmad, M.A., Ahmad Puad, N.A., Bello, O.S., 2014. Kinetic, equilibrium and thermodynamic studies of synthetic dye removal using pomegranate peel activated carbon prepared by microwave-induced KOH activation. Water Resour. Ind. 6, 18–35.

Ayawei, N., Ekubo, A.T., Wankasi, D., Dikio, E.D., 2015. Adsorption of Congo Red by Ni/Al-CO_3: Equilibrium, Thermodynamic and Kinetic Studies. Orient. J. Chem. 31, 1307–1318.

Azzaz, A.A., Khiari, B., Jellali, S., Ghimbeu, C.M., Jeguirim, M., 2020. Hydrochars production, characterization and application for wastewater treatment: A review. Renew. Sustain. Energy Rev. 127, 109882.

Barakan, S., Aghazadeh, V., 2021. The advantages of clay mineral modification methods for enhancing adsorption efficiency in wastewater treatment: a review. Environ. Sci. Pollut. Res. 28, 2572–2599.

Begum, A.S., 2018. Low cost adsorbent as activated carbon for remediation of CU(II) ions from water. International Journal of Research in Pharmacy and Chemistry 8, 450–454.

Biswas, B., Ray, S.K., Majumder, C., 2020. Total organic carbon (TOC) removal from textile wastewater by electro-coagulation: prediction by response surface modeling (RSM). J. Indian Chem. Soc. 97, 2720–2724.

Can, M.E., 2019. Evaluation of animal drinking water quality of cattle enterprises. Fresenius Environ. Bull. 28, 3527–3535.

Chakraborty, B., Roy, S., Shit Pravat, K., Bera, A., Adhikary Partha, P., Bera, B., Sengupta, D., Bhunia Gouri, S., 2021. Eco-restoration of river water quality during COVID-19 lockdown in the industrial belt of eastern India. Environ. Sci. Pollut. Res. Int. 28, 25514–25528.

Chen, A.H., Huang, Y.Y., 2010. Adsorption of Remazol Black 5 from aqueous solution by the templated crosslinked-chitosans. J Hazard Mater 177, 668–675.

Chen, C., Liang, W., Fan, F., Wang, C., 2021. The Effect of Temperature on the Properties of Hydrochars Obtained by Hydrothermal Carbonization of Waste Camellia oleifera Shells. ACS Omega 6, 16546–16552.

Cho, S., Kim, J.-H., Yang, K.S., Chang, M., 2021. Facile preparation of amino-functionalized polymeric microcapsules as efficient adsorbent for heavy metal ions removal. Chem. Eng. J. (Amsterdam, Neth.) 425, 130645.

Dağdelen, S., Acemioğlu, B., Baran, E., Koçer, O., 2014. Removal of Remazol Brilliant Blue R From Aqueous Solution by Pirina Pretreated with Nitric Acid and Commercial Activated Carbon. Water, Air, & Soil Pollution 225.

Donmez, G., 2001. Bioaccumulation of the reactive textile dyes by Candida tropicalis growing in molasses medium. Enzyme Microb. Technol. 30, 4.

Dutta, S., Gupta, B., Srivastava, S.K., Gupta, A.K., 2021. Recent advances on the removal of dyes from wastewater using various adsorbents: a critical review. Materials Advances 2, 4497–4531.

Duttagupta, S., Bhanja, S.N., Dutta, A., Sarkar, S., Chakraborty, M., Ghosh, A., Mondal, D., Mukherjee, A., 2021. Impact of Covid-19 lockdown on availability of drinking water in the arsenic-affected Ganges river basin. Int. J. Environ. Res. Public Health 18, 2832.

Edgar, M., Boyer, T.H., 2021. Removal of natural organic matter by ion exchange: Comparing regenerated and non-regenerated columns. Water Res. 189, 116661.

Ergene, A., Ada, K., Tan, S., Katırcıoğlu, H., 2009. Removal of Remazol Brilliant Blue R dye from aqueous solutions by adsorption onto immobilized Scenedesmus quadricauda: Equilibrium and kinetic modeling studies. Desalination 249, 1308–1314.

Felista, M.M., Wanyonyi, W.C., Ongera, G., 2020. Adsorption of anionic dye (Reactive black 5) using macadamia seed Husks: Kinetics and equilibrium studies. Scientific African 7, e00283.

Fernandes, J.V., Rodrigues, A.M., Menezes, R.R., Neves, G.d.A., 2020. Adsorption of Anionic Dye on the Acid-Functionalized Bentonite. Materials (Basel) 13, 3600.

Foo, K.Y., Hameed, B.H., 2010. Insights into the modeling of adsorption isotherm systems. Chem. Eng. J. 156, 2–10.

Freundlich, H., Helle, W.J., 1939. Ubber die adsorption in Lusungen. J. Am. Chem. Soc. 61, 2–28.

Godiya, C.B., Liang, M., Sayed, S.M., Li, D., Lu, X., 2019. Novel alginate/polyethyleneimine hydrogel adsorbent for cascaded removal and utilization of Cu2+ and Pb2+ ions. J. Environ. Manage. 232, 829–841.

Gómez-Serrano, V., Álvarez, P.M., Jaramillo, J., Beltrán, F.J., 2002. Formation of oxygen complexes by ozonation of carbonaceous materials prepared from cherry stones: I. Thermal effects. Carbon 40, 513–522.

Grcic, I., Koprivanac, N., Andricevic, R., 2017. Reliability study of laboratory scale water treatment by advanced oxidation processes. Environ. Eng. Manage. J. 16, 1–13.

Hartikainen, E.S., Miettinen, O., Hatakka, A., Kahkonen, M.A., 2016. Decolorization of six synthetic dyes by fungi. American J. Environ. Sci. 12, 77–85.

Ho, Y.S., McKay, G., 1999. Pseudo-second order model for sorption processes. Process Biochem. 34, 451–465.

Ho, Y.S., Wase, D.A.J., Forster, C.F., 1996. Kinetic Studies of Competitive Heavy Metal Adsorption by Sphagnum Moss Peat. Environ. Technol. 17, 71–77.

Hu, F., Yang, J., Li, P., Qiu, W., Hou, X., Wei, X., Wang, H., Kauffman, A.E., Xiao, S., Liao, Z., Kimura, S.Y., Zheng, W., Lin, J., Zhu, S., 2021. Is direct-drinking water safe for children An analysis of direct-drinking water quality and its risk factors in Shanghai elementary and middle schools. Int. J. Hyg. Environ. Health 231, 113650.

Jais, F.M., Chee, C.Y., Ismail, Z., Ibrahim, S., 2021. Experimental design via NaOH activation process and statistical analysis for activated sugarcane bagasse hydrochar for removal of dye and antibiotic. J. Environ. Chem. Eng. 9, 104829.

Jawad, A.H., Abdulhameed, A.S., Bahrudin, N.N., Hum, N.N.M.F., Surip, S.N., Syed-Hassan, S.S.A., Yousif, E., Sabar, S., 2021. Microporous activated carbon developed from KOH activated biomass waste: surface mechanistic study of methylene blue dye adsorption. Water Sci. Technol. 84, 1858–1872.

Jawad, A.H., Abdulhameed, A.S., Kashi, E., Yaseen, Z.M., Alothman, Z.A., Khan, M.R., 2022a. Cross-Linked Chitosan-Glyoxal/Kaolin Clay Composite: Parametric Optimization for Color Removal and COD Reduction of Remazol Brilliant Blue R Dye. J. Polym. Environ. 30, 164–178.

Jawad, A.H., Mohammed, I.A., Abdulhameed, A.S., 2020. Tuning of Fly Ash Loading into Chitosan-Ethylene Glycol Diglycidyl Ether Composite for Enhanced Removal of Reactive Red 120 Dye: Optimization Using the Box-Behnken Design. J. Polym. Environ. 28, 2720–2733.

Jawad, A.H., Norrahma, S.S.A., Hameed, B.H., Ismail, K., 2019. Chitosan-glyoxal film as a superior adsorbent for two structurally different reactive and acid dyes: Adsorption and mechanism study. Int. J. Biol. Macromol. 135, 569–581.

Jawad, A.H., Rangabhashiyam, S., Abdulhameed, A.S., Syed-Hassan, S.S.A., Alothman, Z.A., Wilson, L.D., 2022b. Process Optimization and Adsorptive Mechanism for Reactive Blue 19 Dye by Magnetic Crosslinked Chitosan/MgO/Fe_3O_4 Biocomposite. J. Polym. Environ.

Jiang, F., Zhao, W., Wu, Y., Wu, Y., Liu, G., Dong, J., Zhou, K., 2019a. A polyethyleneimine-grafted graphene oxide hybrid nanomaterial: Synthesis and anti-corrosion applications. Appl. Surf. Sci. 479, 963–973.

Jiang, Q., Xie, W., Han, S., Wang, Y., Zhang, Y., 2019b. Enhanced adsorption of Pb(II) onto modified hydrochar by polyethyleneimine or H3PO4: An analysis of surface property and interface mechanism. Colloids Surf., A 583, 123962.

John, Y., David, V.E., Mmereki, D., 2018. A comparative study on removal of hazardous anions from water by adsorption: a review. International Journal of Chemical Engineering, 3975948/3975941-3975948/3975921.

Kavitha, D., Namasivayam, C., 2008. Capacity of activated carbon in the removal of acid brilliant blue: Determination of equilibrium and kinetic model parameters. Chem. Eng. J. 139, 453–461.

Khan, A., Rashid, A., Younas, R., 2015. Adsorption of Reactive Black-5 by Pine Needles Biochar Produced Via Catalytic and Non-catalytic Pyrolysis. Arabian J. Sci. Eng. 40, 1269–1278.

Kharel, G., Sacko, O., Feng, X., Morris, J.R., Phillips, C.L., Trippe, K., Kumar, S., Lee, J.W., 2019. Biochar Surface Oxygenation by Ozonization for Super High Cation Exchange Capacity. ACS Sustain. Chem. Eng. 7, 16410–16418.

Kornaros, M., Lyberatos, G., 2006. Biological treatment of wastewaters from a dye manufacturing company using a trickling filter. J. Hazard. Mater. 136, 95–102.

Lagergren, S., 1898. Handlingar. 24, 1–39.

Langmuir, I., 1918. The adsorption of gases on plane surfaces of glass, mica and platinum. J. Am. Chem. Soc. 40, 1361–1403.

Li, S., Zeng, Z., Xue, W., 2019. Kinetic and equilibrium study of the removal of reactive dye using modified walnut shell. Water Sci Technol 80, 874–883.

Li, T., Tong, Z., Gao, B., Li, Y.C., Smyth, A., Bayabil, H.K., 2020. Polyethyleneimine-modified biochar for enhanced phosphate adsorption. Environ. Sci. Pollut. Res. 27, 7420–7429.

Liu, Q., Gao, J., Li, G., Tao, H., Shi, B., 2019. Accumulation and re-release of metallic pollutants during drinking water distribution and health risk assessment. Environ. Sci. Water Res. Technol. 5, 1371–1379.

Lv, Z., Yang, S., Liu, Y., Zhou, J., Xing, L., Chen, L., 2018. The novel PEI-modified biochars and their application for the efficient elimination of Cr(VI) from aqueous solutions. Water Sci. Technol. 77, 2045–2056.

M.R. Mafra, L.I.-M., D.R. Zuium, E.C. Vasques and M.A. Ferreira, 2012. Adsorption of remazol brilliant blue on an orange peel adsorbent. Brazilian journal of Chemical Engineering 30, 8.

Ma, Y., Liu, W.J., Zhang, N., Li, Y.S., Jiang, H., Sheng, G.P., 2014. Polyethylenimine modified biochar adsorbent for hexavalent chromium removal from the aqueous solution. Bioresour Technol 169, 403–408.

Madduri, S., Elsayed, I., Hassan, E.B., 2020. Novel oxone treated hydrochar for the removal of Pb(II) and methylene blue (MB) dye from aqueous solutions. Chemosphere 260, 127683.

Malek, N.N.A., Jawad, A.H., Abdulhameed, A.S., Ismail, K., Hameed, B.H., 2020. New magnetic Schiff's base-chitosan-glyoxal/fly ash/Fe_3O_4 biocomposite for the removal of anionic azo dye: An optimized process. Int. J. Biol. Macromol. 146, 530–539.

Mate, C.J., Mishra, S., 2020. Synthesis of borax cross-linked Jhingan gum hydrogel for remediation of Remazol Brilliant Blue R (RBBR) dye from water: Adsorption isotherm, kinetic, thermodynamic and biodegradation studies. Int. J. Biol. Macromol. 151, 677–690.

Mengting, Z., Kurniawan, T.A., Avtar, R., Othman, M.H.D., Ouyang, T., Yujia, H., Xueting, Z., Setiadi, T., Iswanto, I., 2021. Applicability of TiO_2(B) nanosheets@hydrochar composites for adsorption of tetracycline (TC) from contaminated water. J. Hazard. Mater. 405, 123999.

Mohd Azmier Ahmada, E.T.C.Y., Ismail Abustanb, Nazwin Ahmadc, Shamsul Kamal, 2011. Optimization of preparations for corn cob based activated carbons for the removal of remazol brilliant blue R dye. International Journal of Engineering & Technology 11, 6.

Mohd Nasir, M.Z., Indiran, G., Ahmad Zaini, M.A., 2021. Assessment of thermal regeneration of spent commercial activated carbon for methylene blue dye removal. Part. Sci. Technol. 39, 504–510.

Munagapati, V.S., Yarramuthi, V., Kim, Y., Lee, K.M., Kim, D.-S., 2018. Removal of anionic dyes (Reactive Black 5 and Congo Red) from aqueous solutions using Banana Peel Powder as an adsorbent. Ecotoxicol. Environ. Saf. 148, 601–607.

Mutembei, K.M., Njogu, E.M., Gichumbi, J.M., 2021. Removal of basic organic dyes from water. J. Chem. Biolog. Phys. Sci. 11, 96–111.

Nair, V., Vinu, R., 2016. Peroxide-assisted microwave activation of pyrolysis char for adsorption of dyes from wastewater. Bioresour Technol 216, 511–519.

Nakamura, H., Oya, M., Hanamoto, T., Nagashio, D., 2017. Reviewing the 20 Years of Operation of Ozonation Facilities in Hanshin Water Supply Authority with Respect to Water Quality Improvements. Ozone Sci. Eng. 39, 397–406.

Ocampo-Perez, R., Padilla-Ortega, E., Medellin-Castillo, N.A., Coronado-Oyarvide, P., Aguilar-Madera, C.G., Segovia-Sandoval, S.J., Flores-Ramírez, R., Parra-Marfil, A., 2019. Synthesis of biochar from chili seeds and its application to remove ibuprofen from water. Equilibrium and 3D modeling. Sci. Total Environ. 655, 1397–1408.

Peers, A.M., 1965. Elovich adsorption kinetics and the heterogeneous surface. J. Catal. 4, 499–503.

Pohl, A., 2020. Removal of Heavy Metal Ions from Water and Wastewaters by Sulfur-Containing Precipitation Agents. Water Air Soil Pollut. 231, 503.

Rafatullah, M., Ahmad, T., Ghazali, A., Sulaiman, O., Danish, M., Hashim, R., 2013. Oil Palm Biomass as a Precursor of Activated Carbons: A Review. Critical Rev. Environ. Sci. Technol. 43, 1117–1161.

Reghioua, A., Barkat, D., Jawad, A.H., Abdulhameed, A.S., Al-Kahtani, A.A., Alothman, Z.A., 2021. Parametric optimization by Box-Behnken design for synthesis of magnetic chitosan-benzil/ZnO/Fe3O4 nanocomposite and textile dye removal. J. Environ. Chem. Eng. 9, 105166.

Roy, S., Tang X Fau - Das, T., Das T Fau - Zhang, L., Zhang L Fau - Li, Y., Li Y Fau - Ting, S., Ting S Fau - Hu, X., Hu X Fau - Yue, C.Y., Yue, C.Y., 2015. Enhanced molecular level dispersion and interface bonding at low loading of modified graphene oxide to fabricate super nylon 12 composites. ACS Applied Materials & Interfaces.

Sajjadi, B., Zubatiuk, T., Leszczynska, D., Leszczynski, J., Chen, W. Y., 2019. Chemical activation of biochar for energy and environmental applications: a comprehensive review. Rev. Chem. Eng. 35, 777–815.

Schroeder, D.W., Guo, W., Missimer, T.M., 2021. Groundwater quality change impacts on a brackish-water reverse osmosis water treatment plant design: the City of Clearwater, Florida. Desalin. Water Treat. 211, 31–44.

Senthilkumar, R., Reddy Prasad, D.M., Govindarajan, L., Saravanakumar, K., Naveen Prasad, B.S., 2018. Improved sorption of reactive black 5 by date seed-derived biochar: isotherm, kinetic, and thermodynamic studies. Sep. Sci. Technol. 54, 2351–2360.

Silva, T.L., Cazetta, A.L., Souza, P.S.C., Zhang, T., Asefa, T., Almeida, V.C., 2018. Mesoporous activated carbon fibers synthesized from denim fabric waste: Efficient adsorbents for removal of textile dye from aqueous solutions. J. Cleaner Prod. 171, 482–490.

Silva, T.L., Ronix, A., Pezoti, O., Souza, L.S., Leandro, P.K.T., Bedin, K.C., Beltrame, K.K., Cazetta, A.L., Almeida, V.C., 2016. Mesoporous activated carbon from industrial laundry sewage sludge: Adsorption studies of reactive dye Remazol Brilliant Blue R. Chem. Eng. J. 303, 467–476.

Sips, R., 1948. On the structure of a catalyst surface. J. Chem. Phys. 16, 490–495.

Sun, S., Jiang, T., Lin, Y., Song, J., Zheng, Y., An, D., 2020. Characteristics of organic pollutants in source water and purification evaluations in drinking water treatment plants. Sci. Total Environ. 733, 139277.

Sun, X.-F., Wang, S.-G., Cheng, W., Fan, M., Tian, B.-H., Gao, B.-Y., Li, X.-M., 2011. Enhancement of acidic dye biosorption capacity on poly(ethylenimine) grafted anaerobic granular sludge. J. Hazard. Mater. 189, 27–33.

Sun, X., Yang, L., Dong, T., Liu, Z., Liu, H., 2016. Removal of Cr(VI) from aqueous solution using amino-modified Fe_3O_4-SiO_2-chitosan magnetic microspheres with high acid resistance and adsorption capacity. J. Appl. Polym. Sci. 133, 43078.

Suzaimi, N.D., Goh, P.S., Malek, N.A.N.N., Lim, J.W., Ismail, A.F., 2019. Performance of branched polyethyleneimine grafted porous rice husk silica in treating nitrate-rich wastewater via adsorption. J. Environ. Chem. Eng. 7, 103235.

Tan, K.B., Vakili, M., Horri, B.A., Poh, P.E., Abdullah, A.Z., Salamatinia, B., 2015. Adsorption of dyes by nanomaterials: Recent developments and adsorption mechanisms. Sep. Purif. Technol. 150, 229–242.

Vijayaraghavan, K., Ashokkumar, T., 2019. Characterization and evaluation of reactive dye adsorption onto Biochar Derived from Turbinaria conoides Biomass. Environ. Prog. Sustainable Energy 38, 13143.

Wang, J., Xie, Q., Li, A., Liu, X., Yu, F., Ji, J., 2020. Biosorption of hexavalent chromium from aqueous solution by polyethyleneimine-modified ultrasonic-assisted acid hydrochar from Sargassum horneri. Water Sci Technol 81, 1114–1129.

Wang, S., Li, Z., Lu, C., 2015. Polyethyleneimine as a novel desorbent for anionic organic dyes on layered double hydroxide surface. J. Colloid Interface Sci. 458, 315–322.

Wang, S., Xiao, K., Mo, Y., Yang, B., Vincent, T., Faur, C., Guibal, E., 2020c. Selenium(VI) and copper(II) adsorption using polyethyleneimine-based resins: Effect of glutaraldehyde crosslinking and storage condition. J. Hazard. Mater. 386, 121637.

Wang, S., Zhen, Z., Tong, Z., Fang, X., Miao, C., 2020d. Decontamination efficiency of phenylethylene by activated carbon-based adsorbent. Nat. Environ. Pollut. Technol. 19, 1663–1668.

Wang, X., Feng, J., Cai, Y., Fang, M., Kong, M., Alsaedi, A., Hayat, T., Tan, X., 2020e. Porous biochar modified with polyethyleneimine (PEI) for effective enrichment of U(VI) in aqueous solution. Sci. Total Environ. 708, 134575.

Wiedner, K., Naisse, C., Rumpel, C., Pozzi, A., Wieczorek, P., Glaser, B., 2013. Chemical modification of biomass residues during hydrothermal carbonization - What makes the difference, temperature or feedstock? Org Geochem. 54, 91–100.

Wong, S., Ghafar, N.A., Ngadi, N., Razmi, F.A., Inuwa, I.M., Mat, R., Amin, N.A.S., 2020. Effective removal of anionic textile dyes using adsorbent synthesized from coffee waste. Sci Rep 10, 2928.

Zhong, Z.-Y., Yang, Q., Li, X.-M., Luo, K., Liu, Y., Zeng, G.-M., 2012. Preparation of peanut hull-based activated carbon by microwave-induced phosphoric acid activation and its application in Remazol Brilliant Blue R adsorption. Ind. Crops Prod. 37, 178–185.